

Peeling limited pedestal experiments in JET-ILW and MAST-U

L. Frassinetti¹, D. King², S. Blackmore², K. Imada³, D. Keeling², C. Perez von Thun⁴, S. Saarelma², C. Giroud², S. Wiesen⁵, A. Kappatou⁶, N. Vianello⁷, E. Alessi⁸, M. Brix², I.S. Carvalho⁹, P. Carvalho⁹, A. Chomiczewska⁴, D. Dunai¹⁰, J. M. Fontdecaba¹¹, E. Giovannozzi¹², J. Harrison², S. Hendersson², D. Kos², B. Labit¹³, M. Lennholm², M. Maslov², A. Meigs², S. Menmuir², R. B. Morales², E. Pawelec¹⁴, G. Pucella¹², R. Scannell², D. Silvagni⁶, A. Stagni⁷, H.J. Sun², D. Terranova⁷, S. Thomas³, JET Contributors*, EUROfusion Tokamak Exploitation Team** and the MAST Upgrade Team***, EUROfusion Consortium, JET, Culham Science Centre, Abingdon, OX14 3DB, UK

¹Division of Electromagnetic Engineering and Fusion Science, KTH Royal Institute of Technology, Stockholm SE, ²UKAEA (United Kingdom Atomic Energy Authority), Culham Campus, Abingdon, Oxfordshire, OX14 3DB, UK, ³York Plasma Institute, Department of Physics, University of York, YO10 5DD, United Kingdom, ⁴Institute of Plasma Physics and Laser Microfusion (IPPLM), Hery 23, 01-497 Warsaw, Poland, ⁵DIFFER - Dutch Institute for Fundamental Energy Research, 5612 AJ Eindhoven, The Netherlands, ⁶Max-Planck-Institut für Plasma Physik, Boltzmannstr.2, 85748 Garching, Germany, ⁷Consorzio RFX, Corso Stati Uniti 4, 35127 Padova, Italy, ⁸Institute for Plasma Science and Technology, CNR, 20125 Milano, Italy, ⁹ITER Organization, Route de Vinon-sur-Verdon, CS 90 046, 13067 St Paul Lez Durance Cedex, France, ¹⁰Centre for Energy Research, Budapest, Hungary, ¹¹Laboratorio Nacional de Fusión, CIEMAT, Madrid, Spain, ¹²Fusion and Nuclear Safety Department - ENEA C. R. Frascati - Frascati (Roma), Italy, ¹³Ecole Polytechnique Fédérale de Lausanne (EPFL), Swiss Plasma Center (SPC), Lausanne, Switzerland, ¹⁴Institute of Physics, University of Opole, Poland, *See the author list of CF. Maggi et al., Nucl. Fusion 2024, 10.1088/1741-4326/ad3e16, **see the author list of E. Joffrin Nuclear Fusion 2024 10.1088/1741-4326/ad2be4 ** see author list of J.R. Harrison et al 2019 Nucl. Fusion 59 112011.

1. Introduction.

ITER will operate at low pedestal collisionality ($\nu_{ee}^{*ped} < 0.1$) and at high separatrix density (n_e^{sep}). In these ν_{ee}^{*ped} ranges, the ITER pedestal will be limited by peeling instabilities. The pedestal properties, for example the correlation of the pedestal pressure with the pedestal top density (n_e^{ped}) and n_e^{sep} , are supposed to be different between peeling and ballooning limited plasmas. Since the European machines commonly operate at the ballooning boundary, validation of ITER pedestal predictions have been relied only on DIII-D results [1].

The goal of this work is to (1) reach peeling limited pedestals in JET and MAST-U, (2) test the pedestal behavior with n_e^{ped} and n_e^{sep} in JET and MAST-U peeling limited pedestals and (3) test the pedestal predictive capabilities in peeling limited plasmas.

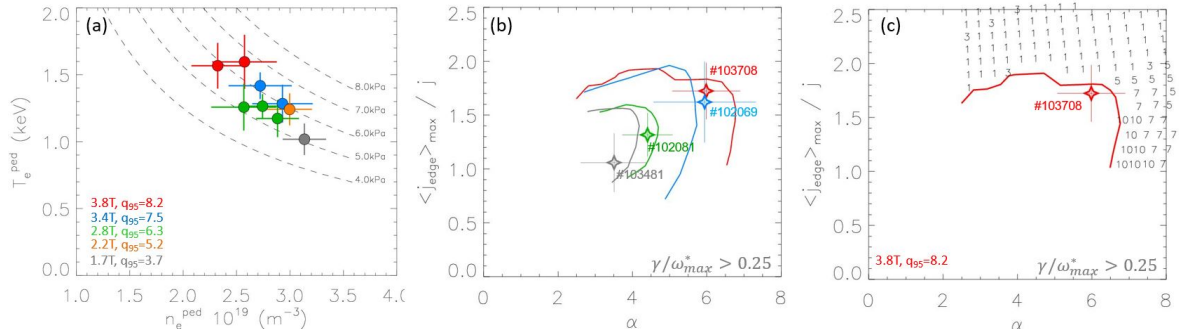


Figure 1. (a) JET-ILW pre-ELM T_e^{ped} and n_e^{ped} for the q_{95} scan at constant engineering parameters. (b) PB stability diagram for selected pulse from the JET-ILW q_{95} scan. The diamagnetic criterion has been used to define the stability boundary. The use of the Alfvén criterion leads to similar results. (c) PB stability diagram for the JET-ILW $q_{95}=8.2$ pulse #103708. The numbers highlight the most unstable mode.

2. Reaching peeling limited pedestals in JET-ILW.

Europed [2] predictive modelling suggests that, within the achievable ranges of JET-ILW engineering parameters, peeling limited plasmas can be achieved only at $q_{95} > 7-8$, low density and low ν^* . To reach low density and low ν^* , we have used a scenario characterized by low I_p (1.4MA), outer strike point on the divertor corner (near the vacuum pump duct), low gas rate ($\Gamma_D = 0.1 \times 10^{22} \text{ (e/s)}$) and high input power ($P_{aux} = 25 \text{ MW}$ composed of $P_{nbi} = 22-23 \text{ MW}$ and $P_{ICRH} = 2-3 \text{ MW}$ which, in the achieved density range, is the maximum power compatible with no shine-through and no reionization issues). High triangularity shape ($\langle \delta \rangle \approx 0.39$) has been used to be more ITER-relevant. To reach peeling limited pedestals a q_{95} scan, performed at constant engineering parameters and at gas rate $\Gamma_D = 0.7-1.1 \times 10^{22} \text{ (e/s)}$, has been done. The q_{95} scan is done by increasing B_t shot by shot, from $B_t = 1.7 \text{ T}$ and $q_{95} = 3.7$ to $B_t = 3.8 \text{ T}$ and $q_{95} = 8.2$. The corresponding pre-ELM pedestal temperature (T_e^{ped}) and density (n_e^{ped}) are shown in

figure 1(a). The increasing q_{95} leads to a decreasing n_e^{ped} and an increasing T_e^{ped} (up to 1.5-1.6keV), with a weak increase in the pre-ELM pedestal pressure (p_e^{ped}). The peeling-balloning (PB) stability analysis for four selected pulses in the q_{95} scan is shown in figure 1(b). The PB stability analysis is done with HELENA for the equilibrium and MISHKA for the stability, using the Redl formula for the bootstrap current (j_{bs}) and including the toroidal modes $n=1,2,5,7,10,20,30,50$. The PB stability diagram shows that the pedestal is at the ballooning boundary at $q_{95}=3.7$ and it reaches the corner of the PB stability boundary at $q_{95}=7.5$. At $q_{95}=8.2$ the pedestal reaches the peeling boundary and is limited by low- n peeling modes ($n=1-5$) as shown in figure 1(c). In the rest of the work, only the peeling limited $q_{95}=8.2$ scenario is used.

3. Reaching peeling limited pedestals in MAST-U.

Peeling limited pedestal in MAST-U have been reached by high power operation and by using an optimized plasma shape with high triangularity and high elongation. The details of the optimization are discussed in reference [3]. The MAST-U scenario used in this work, and established in reference [3], is characterized by $I_p=750\text{kA}$, $B_t=0.5\text{T}$, $q_{95}=6.7$, $P_{NBI}=3.2\text{MW}$, $\langle\delta\rangle\approx 0.49$ and elongation $\kappa=2.1$. The PB stability diagram for pulse #49109 performed with gas rate $\Gamma_D=0.1\times 10^{22}(\text{e/s})$ is shown in figure 2. The same stability work-flow used for JET-ILW has been employed. Figure 2(a) shows the stability boundary determined using the Alfvén criterion ($\gamma/\omega_A=0.03$). The pedestal is at the corner of the PB stability boundary and, within the uncertainties, the most unstable modes are either low- n peeling modes ($n=3$) or high- n ballooning modes ($n=30$). Figure 2(b) shows the stability boundary using the diamagnetic criterion ($\gamma/\omega^*_{max}=0.25$). In this case, the pedestal is fully at the peeling boundary with pedestal limited by the low- n peeling modes ($n=1-2$). The difference between the two criteria is due to the fact that the ballooning modes in figure 2(a) are very weak and the diamagnetic criterion stabilizes them very easily.

4. The JET-ILW and MAST-U datasets.

The JET-ILW $q_{95}=8.2$ scenario described in section 2 and the MAST-U scenario described in section 3 have been used. Starting from the reference pulses described in sections 2 and 3, a gas rate scan has been performed in both machines. The goal of the gas rate scan is to reach a variation in n_e^{ped} and/or n_e^{sep} . As shown in figure 3(a), the increasing gas rate leads to an increasing ELM frequency (f_{ELM}). Till $f_{ELM}\approx 70\text{Hz}$, the increasing ELM frequency leads to a weak decrease in n_e^{ped} , as shown in figure 3(b). The reason of the decrease is still under investigation and the current hypothesis is an increase in the ELM

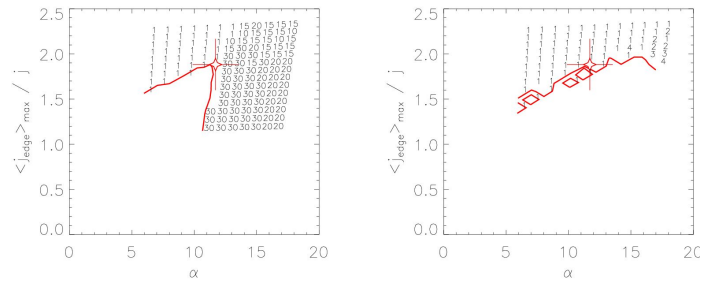


Figure 2. PB stability diagram for the MAST-U pulse #49108. In frame (a) the stability boundary is determined using the Alfvén criterion and in frame (b) using the diamagnetic criterion.

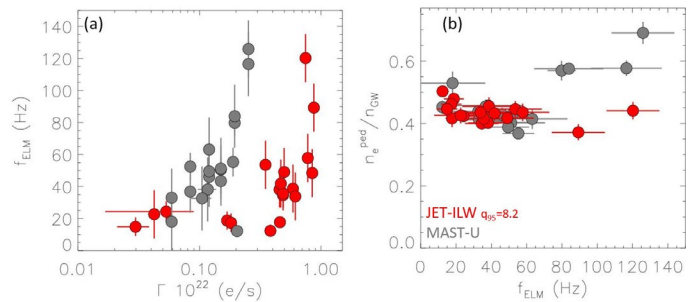


Figure 3. (a) ELM frequency versus gas rate and (b) ratio between n_e^{ped} and Greenwald density versus ELM frequency for the datasets used in section 5.

particle losses due to the increased f_{ELM} . Above 70Hz, no variation in JET-ILW n_e^{ped} is observed while a significant increase in the MAST-U n_e^{ped} occurs.

The achieved ranges of collisionality and n_e^{sep}/n_e^{ped} are shown in figure 4. In the MAST-U dataset, ν_{ee}^{*ped} down to ≈ 0.3 has been reached, with n_e^{sep}/n_e^{ped} in the range 0.4-0.9. The four MAST-U pulses with $f_{ELM} > 70\text{Hz}$ are characterized by a much higher collisionality, with $\nu_{ee}^{*ped} \approx 2$ and $n_e^{sep}/n_e^{ped} > 0.8$. The JET-ILW dataset has reached collisionality down to $\nu_{ee}^{*ped} \approx 0.15$ and n_e^{sep}/n_e^{ped} in the range 0.35-0.8. In terms of $\nu_{ee}^{*ped} - n_e^{sep}/n_e^{ped}$, JET-ILW is approaching a ITER relevant range. As reference, the empty triangles represent all the high- δ JET-ILW plasmas achieved till 2022 and extracted from the JET EUROfusion database [4]. The JET-ILW $q_{95}=8.2$ scenario has reached ν_{ee}^{*ped} significantly lower than any JET-ILW high- δ plasmas achieved before 2022.

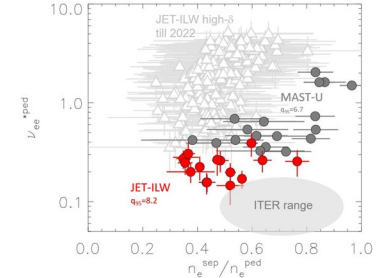


Figure 4. ν_{ee}^{*ped} and n_e^{sep}/n_e^{ped} for the JET-ILW and MAST-U datasets.

5. Pedestal pressure behavior.

The pre-ELM electron pedestal pressure versus the pedestal density is shown in figure 5(a) and 5(b) for the JET-ILW dataset and the MAST-U dataset. In the JET-ILW dataset, a clear positive correlation between p_e^{ped} and n_e^{ped} is present. The same correlation holds also for p_i^{ped} (not shown here).

In the MAST-U dataset, a positive correlation between p_e^{ped} and n_e^{ped} can be seen till $n_e^{ped} \approx 4.3 \times 10^{19} \text{m}^{-3}$. Above this density, a significant drop in the pressure can be observed. The pulses at $n_e^{ped} > 4.3 \times 10^{19} \text{m}^{-3}$ corresponds to the $f_{ELM} > 70\text{Hz}$ MAST-U pulses in figure 3(b) and the $\nu_{ee}^{*ped} \approx 2$ pulses in figure 4.

A preliminary analysis has not identified any significant difference in impurity content below and above $n_e^{ped} \approx 4.3 \times 10^{19} \text{m}^{-3}$. So, the p_e^{ped} drop in the MAST-U dataset might be due either to a transition to type III ELMs or to a transition to ballooning limited pedestals. At this stage other reasons for the p_e^{ped} drop cannot be excluded.

In both datasets, the increasing p_e^{ped} with increasing n_e^{ped} is due to a widening of the pedestal width, as shown in figures 5(c) and 5(d). This is very clear especially for the MAST-U dataset, in which the pressure width increases from $w_{pe} \approx 0.035 \psi_N$ at $n_e^{ped} \approx 3 \times 10^{19} \text{m}^{-3}$ to $w_{pe} \approx 0.07 \psi_N$ at $n_e^{ped} \approx 4.2 \times 10^{19} \text{m}^{-3}$. This behavior is consistent with what observed in TCV peeling limited scenario, as earlier described in reference [5].

The positive correlation observed in the JET-ILW dataset and in the MAST-U dataset (at $n_e^{ped} < 4.3 \times 10^{19} \text{m}^{-3}$) is opposite to what typically observed in European machines, which mainly operate with the pedestal at the ballooning boundary, as discussed for example in AUG [6] and JET [7].

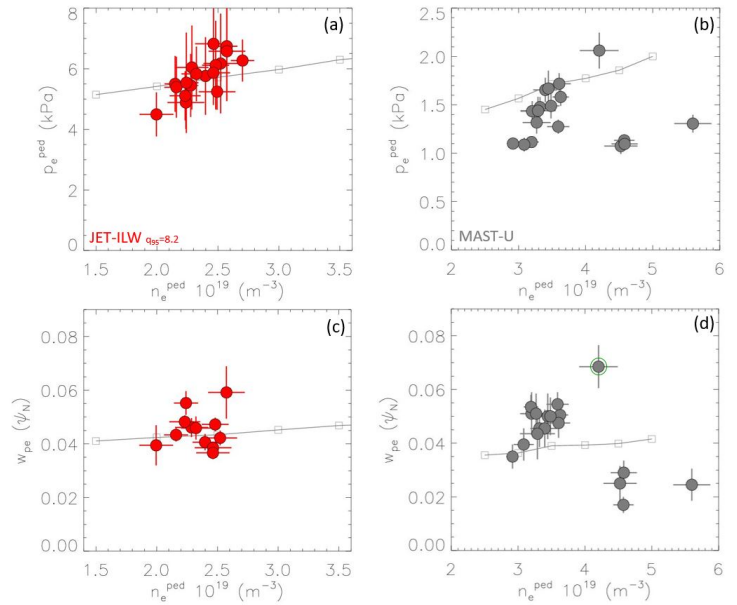


Figure 5. Pre-ELM p_e^{ped} vs n_e^{ped} in the JET-ILW $q_{95}=8.2$ dataset (a) and in the MAST-U dataset (b). Pressure width vs n_e^{ped} for the JET-ILW dataset (c) and the MAST-U dataset (d). The continuous lines and the squares show the European predictions (discussed in section 6).

Since ITER will operate in peeling limited pedestal scenarios at high n_e^{sep}/n_e^{ped} , to reach reliable pedestal predictions in ITER it is important to assess how p_e^{ped} is correlated to n_e^{sep}/n_e^{ped} in the JET-ILW and MAST-U datasets. The correlation is shown in figure 6. Since the pedestal pressure is strongly correlated to n_e^{ped} (figure 5), figure 6 shows subsets characterized by similar density, $n_e^{ped}=2.2-2.4 \times 10^{19}$ for the JET-ILW dataset and $n_e^{ped}=3.3-3.7 \times 10^{19}$ for the MAST-U dataset. No strong correlation can be seen. This is different to what observed at the ballooning boundary, where clear negative correlations have been observed in earlier works [6,7] and it is a good news for ITER as no pedestal degradation at high n_e^{sep}/n_e^{ped} can be expected.

6. Pedestal predictions.

The p_e^{ped} experimental trends have been compared with Europed predictions [2] using HELENA and MISHKA. The input parameters β_N , n_e^{ped} and relative shift corresponds to the values of a reference pulse from the JET-ILW dataset and from the MAST-U dataset (figure 1(c) and figure 2). For JET, the standard KBM constant has been used ($w=0.076(\beta_0^{ped})^{0.5}$) while for MAST-U the KBM constant determined in [8] has been used ($w=0.10(\beta_0^{ped})^{0.5}$).

First, a n_e^{ped} scan has been performed keeping all other input parameters constant. The results is shown by continuous lines in figure 5. The Europed scans predict a positive correlation between p_e^{ped} and n_e^{ped} . Qualitatively, the predictions are in agreement with the experimental trends. Quantitatively, disagreement might be due to the fact that all input parameters apart from n_e^{ped} have been kept constant.

Second, a scan in the relative shift has been performed to change n_e^{sep}/n_e^{ped} while keeping the other input parameters constant. As shown by the continuous lines in figure 6, Europed does not predict any significant variation of p_e^{ped} with n_e^{sep}/n_e^{ped} , in good agreement with the experimental results.

7. Conclusions

Peeling limited pedestals have been reached both in JET-ILW and MAST-U. In both machines, a positive correlation between p_e^{ped} and n_e^{ped} has been observed and no strong degradation of p_e^{ped} with increasing n_e^{sep}/n_e^{ped} is present. Europed modelling shows good qualitative agreement with experimental results.

Acknowledgements

This research is supported by Vetenskapsrådet under Grant No. 2023-04895. This work has been carried out within the framework of the EUROfusion Consortium, funded by the European Union via the Euratom Research and Training Programme (Grant Agreement No 101052200 — EUROfusion) and from the EPSRC [grant number EP/W006839/1]. Views and opinions expressed are however those of the author(s) only and do not necessarily reflect those of the European Union or the European Commission. Neither the European Union nor the European Commission can be held responsible for them. The Swiss contribution to this work has been funded by the Swiss State Secretariat for Education, Research and Innovation (SERI). Views and opinions expressed are however those of the author(s) only and do not necessarily reflect those of the European Union, the European Commission or SERI. Neither the European Union nor the European Commission nor SERI can be held responsible for them.

REFERENCES

- | | |
|--|--|
| [1] Snyder P. et al., Nucl. Fusion 55, 083026 (2015) | [5] Frassinetti L. et al., O4.108, 48th EPS (2022) |
| [2] Saarelma S et al., Phys. Plasmas 26, 072501 (2019) | [6] Dunne M. et al., PPCF 59, 025010 (2017) |
| [3] K. Imada et al., Nucl. Fusion 64, 086002 (2024) | [7] Frassinetti L. et al. Nucl. Fusion 61, 126054 (2021) |
| [4] Frassinetti L. et al. Nucl. Fusion 61, 016001 (2021) | [8] Smith S. et al., Plasma Phys. Control. Fusion 64 (2022) 045024 |

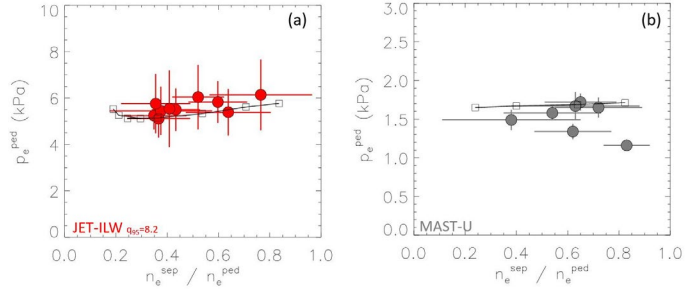


Figure 6. Pre-ELM p_e^{ped} vs n_e^{sep}/n_e^{ped} in the JET-ILW $q_{95}=8.2$ dataset (a) and in the MAST-U dataset (b). The continuous lines show the Europed predictions.